Application of Novel Batteries of TM-doped Nitride-based Materials towards Clean Energy Storage: A DFT Study

Fatemeh Mollaamin [a]*, Majid Monajjemi [b]

[a] Department of Biomedical Engineering, Faculty of Engineering and Architecture, Kastamonu University, Kastamonu, Turkey.

[b] Department of Chemical Engineering, Central Tehran Branch, Islamic Azad University, Tehran, Iran.

Aplicación de nuevas baterías de materiales a base de nitruro dopados con TM para el almacenamiento de energía limpia: un estudio DFT

Aplicació de noves bateries de materials basats en nitrur dopats amb TM cap a l'emmagatzematge d'energia neta: un estudi DFT

RECEIVED: 29 OCTOBER 2024; ACCEPTED: 27 MARCH 2025 HTTPS://DOI.ORG/10.55815/431847

ABSTRACT

The Mn-doped GaN-based nanomaterials indicate strong dynamic stability which results in a half-metallicity property. This article aims to investigate the hydrogen grabbing by heteroclusters of Mn-doped GaN, AlGaN, InGaN was carried out using DFT computations at the CAM–B3LYP–D3/6–311+G (d,p) level of theory. The notable fragile signal intensity close to the parallel edge of the nanocluster sample might be owing to manganese binding induced non-spherical distribution of MnGaN, MnAlGaN or MnInGaN heteroclusters. The hypothesis of the energy adsorption phenomenon was confirmed by density distributions of CDD, DOS/TDOS, and ESP for GaN and its alloys. Based on DOS/TDOS, the excessive growth technique on doping manganese is a potential approach to designing high efficiency hybrid semipolar gallium nitride-based devices in a long wavelength zone. A vaster jointed area engaged by an isosurface map for Mn doping GaN, AlGaN, InGaN towards formation of nanocomposites of MnGaN–H, MnAlGaN–H, MnInGaN–H after hydrogen adsorption due to labeling atoms of N(4), Mn(5), H (18), respectively. Therefore, it can be considered that manganese in the functionalized MnGaN, MnAlGaN or MnInGaN might have more impressive sensitivity for accepting the electrons in the process of hydrogen adsorption. Furthermore, MnGaN, MnAlGaN or MnInGaN are potentially advantageous for certain high-frequency applications requiring batteries for energy storage. These results indicate the controllability and variability of two-dimensional GaN-based materials, providing new avenues for the potential use of GaN as a material for optoelectronic devices and batteries. The Mn impurities can help improve the value of semiconductors compared to intrinsic GaN material. This research result has significance for the application of GaN based semiconductor materials in thermoelectric fields.

Keywords: Sustainable batteries; safe energy saving; green chemistry; eco-friendly nanocomposites

RESUMEN

Los nanomateriales basados en GaN dopado con Mn presentan una fuerte estabilidad dinámica, lo que les confiere una propiedad de semimetalicidad. Este artículo tiene como objetivo investigar la captación de hidrógeno por heterocúmulos de GaN, AlGaN e InGaN dopados con Mn mediante cálculos DFT en el nivel teórico CAM–B3LYP–D3/6–311+G (d,p). La notable fragilidad de la intensidad de la señal cerca del borde paralelo de la muestra del nanocúmulo podría deberse a la distribución no esférica inducida por la unión del manganeso de los heterocúmulos de MnGaN, MnAlGaN o MnInGaN. La hipótesis del fenómeno de adsorción de energía se confirmó mediante las distribuciones de densidad de CDD, DOS/TDOS y ESP para GaN y sus aleaciones. Basada en DOS/TDOS,

*Corresponding author: fmollaamin@kastamonu.edu.tr

la técnica de crecimiento excesivo sobre el dopaje de manganeso constituye un enfoque potencial para el diseño de dispositivos híbridos semipolares de alta eficiencia basados en nitruro de galio en una zona de longitud de onda larga. Un área de unión más amplia, comprometida por un mapa de isosuperficie para el dopaje con Mn de GaN, AlGaN e InGaN, conduce a la formación de nanocompuestos de MnGaN–H, MnAlGaN–H y MnInGaN–H tras la adsorción de hidrógeno, gracias al marcaje de átomos de N(4), Mn(5) y H(18), respectivamente. Por lo tanto, se puede considerar que el manganeso en los MnGaN, MnAlGaN o MnInGaN funcionalizados podría presentar una mayor sensibilidad para la aceptación de electrones en el proceso de adsorción de hidrógeno. Además, los MnGaN, MnAlGaN o MnInGaN son potencialmente ventajosos para ciertas aplicaciones de alta frecuencia que requieren baterías para el almacenamiento de energía. Estos resultados indican la controlabilidad y variabilidad de los materiales bidimensionales basados en GaN, lo que abre nuevas posibilidades para su uso como material para dispositivos optoelectrónicos y baterías. Las impurezas de Mn pueden contribuir a mejorar el valor de los semiconductores en comparación con el material de GaN intrínseco. Este resultado de investigación tiene importancia para la aplicación de materiales semiconductores basados en GaN en campos termoeléctricos.

Palabra clave: Baterías sostenibles; ahorro energético seguro; química verde; nanocompuestos ecológicos

RESUM

Els nanomaterials basats en GaN dopats amb Mn indiquen una forta estabilitat dinàmica que resulta en una propietat de mitja metal·licitat. Aquest article pretén investigar la captura d'hidrogen per heterocúmuls de GaN, AlGaN, InGaN dopats amb Mn es va dur a terme mitjançant càlculs DFT al nivell de teoria CAM-B3LYP-D3/6-311 + G (d, p). La notable intensitat del senyal fràgil propera a la vora paral·lela de la mostra del nanocluster podria ser deguda a la distribució no esfèrica induïda per la unió de manganès dels heterocúmuls MnGaN, MnAlGaN o MnInGaN. La hipòtesi del fenomen d'adsorció d'energia es va confirmar mitjançant distribucions de densitat de CDD, DOS/TDOS i ESP per a GaN i els seus aliatges. Basat en DOS/TDOS, la tècnica de creixement excessiu del dopatge de manganès és un enfocament potencial per dissenyar dispositius híbrids basats en nitrur de gal semipolar d'alta eficiència en una zona de longitud d'ona llarga. Una àrea articulada més àmplia implicada per un mapa isosuperfície per al dopatge de Mn GaN, AlGaN, InGaN cap a la formació de nanocomposites de MnGaN–H, MnAlGaN–H, MnInGaN–H després de l'adsorció d'hidrogen a causa de l'etiquetatge d'àtoms de N (4), Mn (5), H (18), respectivament. Per tant, es pot considerar que el manganès en el MnGaN, MnAlGaN o MnInGaN funcionalitzat podria tenir una sensibilitat més impressionant per acceptar els electrons en el procés d'adsorció d'hidrogen. A més, MnGaN, MnAlGaN o MnInGaN són potencialment avantatjoses per a determinades aplicacions d'alta freqüència que requereixen bateries per a l'emmagatzematge d'energia. Aquests resultats indiquen la controlabilitat i la variabilitat dels materials bidimensionals basats en GaN, proporcionant noves vies per a l'ús potencial de GaN com a material per a dispositius optoelectrònics i bateries. Les impureses de Mn poden ajudar a millorar el valor dels semiconductors en comparació amb el material intrínsec de GaN. Aquest resultat de la investigació té importància per a l'aplicació de materials semiconductors basats en GaN en camps termoelèctrics.

Paraules clau: bateries sostenibles; estalvi energètic segur; química verda; nanocomposites ecològics

1. INTRODUCTION

It is well known that doping can adjust the electronic properties of GaN materials, such as carrier concentration, carrier mobility, and electronic band structure. A binary III/V direct bandgap semiconductor called Gallium nitride (GaN) is a very hard material with wide bandgap applied in a variety of technologies, including optoelectronic, high-power electronics and light-emitting diodes, partly due to its favorable thermal properties [1,2]. The nitrides of group III in periodic table have low sensitivity to ionizing radiation which make them appropriate materials for solar cell arrays for satellites. Therefore, space applications could also benefit as devices have shown stability in high radiation environments.

Ternary "AlGaN" alloys have been recognized as promising materials for realizing deep ultraviolet "DUV" optoelectronic devices with operating wavelengths down to 200 nm [1–3]. For the development of high performance AlGaN-based "DUV" devices, high-conductivity p-type Al-rich $Al_xGa_{1-x}N$ ($x \geq 0.4$) is essential. Many studies have shown that enhancing the p-type conductivity

has a significant effect on the improvement of both the electrical and optical properties of AlGaN DUV optoelectronics [4–8]. In an investigation, the scientists have shown the $Al_{0.1}Ga_{0.9}N$/GaN heterojunction solar cells with a Mn-doped active layer. Under a 1-sun AM1.5 G illumination condition, the devices exhibited an improved conversion efficiency by a magnitude of 5 compared to the cells without Mn doping in the active layer. This dramatic increase in conversion efficiency is attributed to the fact that the Mn-related energy states cause sub-band gap photon absorption and thereby contribute an extra photocurrent [9]. The investigations conducted on Mn-doped GaN have shown that the Mn impurity band could form approximately at the middle of the GaN band gap [10].

The researchers have estimated the suitability of Mn doped $In_{1-x}Ga_xN$ as an IB material. They predicted that the $In_{1-x}Ga_xN$-based solar cells with an Mn-doped absorption layer could achieve maximum efficiency [11].

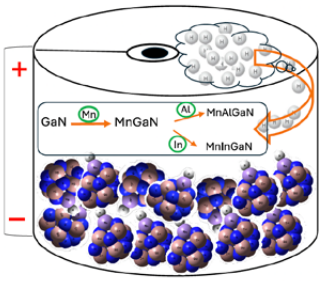

Figure 1. *Application of Mn-doped hetero-clusters of GaN, AlGaN, InGaN for hydrogen storage in transistors using CAM–B3LYP–D3/6-311+G (d,p) calculation.*

The ternary semiconductor of Indium gallium nitride (InGaN) as solar cells is remarkable owing to the adjustable direct band gap energy of InGaN veiling the total solar spectrum arraying from 0.7 to 3.4 eV [12,13], as well as preferable photovoltaic specifics of InGaN consisting of vast absorption coefficients [14] and high carrier dynamism. Furthermore, great fixity and excellent radiation persistence of InGaN alloys permit function of InGaN-based instruments in uttermost situations such as space and geocentric usages [12,15]. The solar cells of InGaN were constructed with low indium amounts of the InGaN alloy compounds [16–18] which conduces to an enhancement in the band gap energy of InGaN and then eventuates in the absorption of shorter wavelengths of solar radiation. Therefore, to find out InGaN solar cells with high yield, the In amount in the InGaN active layer of these solar cells should be enhanced to compensate a large part of the solar spectrum. Recently, it has been suggested the application of dual nanogratings of Si and other organic solar cells which are mostly in direct contact with the active area of the solar cells [19–25]. Moreover, the researchers fabricated transition metal zinc doped InGaN nanorods arrays by radio-frequency plasma-assisted molecular beam epitaxy. Doping obviously reduces indium atoms composition, the aggregation of In–In and induces the deep energy level. This greatly decreases the defects and improves the valence band potential of InGaN nanorods [26].

Recently, researchers have proposed an InGaN/GaN p-i-n thin-film solar cell which includes a dual nanograting compound: silver nanogratings on the back of the solar cell and GaN-NGs on the front. FDTD simulation parameters have exhibited that the dual NG compound connects the eventual sunlight to the plasmonic and photonic styles, so enhancing the absorption of the solar cell in a wide spectral span. It is perceived that the solar cells possessing the double nanograting structures have a considerable increment in light absorption compared with cells having either no nanogratings or having only the front nanogratings or only the back nanogratings [27].

In this paper, we propose the feasible semiconductors of GaN, AlGaN, InGaN which are doped with manganese. We carried out molecular modelling considering the geometrical parameters of doping atoms on the surface of MnGaN, MnAlGaN, MnInGaN through hydrogen absorption status and current charge density of the batteries was studied (Figure 1). Moreover, the effect of a relative chemical shift between GaN, AlGaN, InGaN and doped heteroclusters of the batteries was also investigated. Mn doping can transform GaN materials into p-type semiconductors, which is crucial for achieving p-n junctions or p-type layers in GaN based electronic devices. The first study helps us investigate the physical properties exhibited by different atoms in Mn substituted GaN at high doping concentrations.

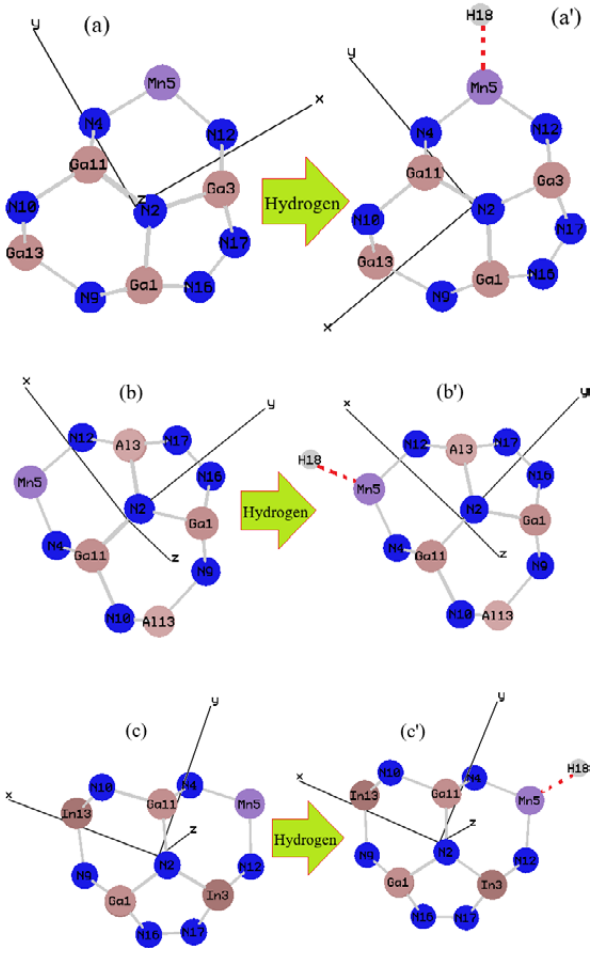

Figure 2. *Characterization of heteroclusters include* **(a)** *MnGaN,* **(a')** *MnGaN–H,* **(b)** *MnAlGaN,* **(b')** *MnAlGaN–H,* **(c)** *MnInGaN,* **(c')** *MnInGaN–H through a labeled ring towards H-adsorption.*

2. THEORETICAL BACKGROUNDS AND APPROACHES

The Mn-doped GaN, AlGaN, InGaN nanocomposites were calculated within the framework of first-principles calculation based on density functional theory (DFT) (Figure 2a,a',b,b',c,c'). The rigid potential energy surface using density functional theory [28–41] was performed due to Gaussian 16 revision C.01 program package [42] and GaussView 6.1 [43]. The coordination input for energy storage on the batteries has applied basis sets of 6–311+G (d,p) and EPR–3 in conjunction with a chosen DFT functional of CAM–B3LYP–D3 with

multiplicity 2 for MnGaN, MnAlGaN, MnInGaN and multiplicity 1 for MnGaN–H, MnAlGaN–H, MnInGaN–H nanoclusters. Electron paramagnetic resonance (EPR) is defined as the form of spectroscopy concerned with microwave-induced transitions between magnetic energy levels of electrons having a net spin and orbital angular momentum. Furthermore, the nuclear quadrupole resonance (NQR) frequencies have been measured for MnGaN, MnAlGaN, MnInGaN towards estimating the hydrated nanocluster of MnGaN–H, MnAlGaN–H, MnInGaN–H (Table 1a,b,c). The NQR method is related to the multipole expansion in Cartesian coordinates as the equation (1) [44,45]:

$$V(r) = V(0) + \left[\left(\frac{\partial V}{\partial x_i}\right)\Big|_0 . x_i\right] + \frac{1}{2}\left[\left(\frac{\partial^2 V}{\partial x_i x_j}\right)\Big|_0 . x_i x_j\right] + \cdots \quad (1)$$

After that, a simplification on the equation (1), there are only the second derivatives related to the identical variable for the potential energy [44–47]:

$$U = -\frac{1}{2}\int_{\mathcal{D}} d^3 r\, \rho_r \left[\left(\frac{\partial^2 V}{\partial x_i^2}\right)\Big|_0 . x_i^2\right] = -\frac{1}{2}\int_{\mathcal{D}} d^3 r\, \rho_r \left[\left(\frac{\partial E_i}{\partial x_i}\right)\Big|_0 . x_i^2\right] = -\frac{1}{2}\left(\frac{\partial E_i}{\partial x_i}\right)\Big|_0 . \int_{\mathcal{D}} d^3 r\, [\rho(r) . x_i^2] \quad (2)$$

First, we optimized the structural parameters of nanoclusters of GaN, AlGaN, InGaN which are doped with manganese towards formation of heteroclusters of MnGaN, MnAlGaN, MnInGaN for obtaining the highest short-circuit current density. Then, Figure 2(a,a',b,b',c,c') shows the process of hydrogen adsorption on heteroclusters of MnGaN, MnAlGaN, MnInGaN which are varied to maximize the absorption in the active region. Since ring area and perimeter are sometimes involved in wave function analysis, they need to be calculated. In this function, it is needed to input the index of the atoms in the ring in clockwise manner including Mn5, N12, Ga6, N7, Ga15, N4 (Figure2a,a',b,b',c,c'). Then, it has be calculated the total ring area and total ring perimeter for a tailored ring as 9.6981Å and 11.6921 Å^2, respectively (Figure2 a,a',b,b',c,c'). GaN materials with different Mn doping concentrations were calculated. For strongly correlated systems containing d and f orbital electrons, there is a strong in situ Coulomb interaction between electrons. The generalized gradient approximation (GGA) in the exchange-correlation functional does not accurately describe the strong in situ Coulomb interaction between electrons, so the band gap value is often underestimated in the calculation process [48].

Table 1. *The electric potential (E_p/a.u.) and Bader charge (Q/coulomb) through NQR calculation for selected atoms of* **(a)** *MnGaN/MnGaN–H,* **(b)** *MnAlGaN/MnAlGaN–H,* **(c)** *MnInGaN/MnInGaN –H heteroclusters.*

(a)

MnGaN			MnGaN–H		
Atom	Q	E_p	Atom	Q	E_p
Ga(1)	0.9961	−1.2490	Ga(1)	1.0084	−1.2238
N(2)	−1.0483	−18.408	N(2)	−1.0386	−18.391
Ga(3)	0.9744	−1.2497	Ga(3)	0.9936	−1.2285
N(4)	−1.0171	−18.4093	N(4)	−0.9210	−18.3993
Mn(5)	0.7522	−16.6505	Mn(5)	0.4224	−16.6378
Ga(6)	0.9743	−1.2497	Ga(6)	0.9933	−1.2267
N(7)	−1.0482	−18.4083	N(7)	−1.0490	−18.3864
Ga(8)	0.9958	−1.2490	Ga(8)	1.0123	−1.2224
N(9)	−1.0455	−18.4122	N(9)	−1.0148	−18.3901
N(10)	−0.6809	−18.4169	N(10)	−0.6763	−18.3855
Ga(11)	1.0012	−1.2522	Ga(11)	1.0242	−1.2392
N(12)	−0.9800	−18.4081	N(12)	−0.9025	−18.3842
Ga(13)	0.9259	−1.2537	Ga(13)	0.9193	−1.2418
N(14)	−0.6808	−18.4169	N(14)	−0.6916	−18.3896
Ga(15)	1.0012	−1.2522	Ga(15)	1.0272	−1.2358
N(16)	−0.5692	−18.3631	N(16)	−0.5456	−18.3231
N(17)	−0.5512	−18.3641	N(17)	−0.5327	−18.3222
-	-	-	H(18)	−0.0285	−1.1338

(b)

MnAlGaN			MnAlGaN–H		
Atom	Q	E_p	Atom	Q	E_p
Ga(1)	0.9852	−1.2503	Ga(1)	0.9958	−1.2238
N(2)	−1.1478	−18.4129	N(2)	−1.1288	−18.391
Al(3)	1.2520	−1.2192	Al(3)	1.2506	−1.2285
N(4)	−1.0561	−18.4182	N(4)	−0.9446	−18.3993
Mn(5)	0.7651	−16.6575	Mn(5)	0.3908	−16.6378
Ga(6)	0.9729	−1.2503	Ga(6)	0.9814	−1.2267
N(7)	−1.1444	−18.4122	N(7)	−1.1129	−18.3864
Al(8)	1.2493	−1.2188	Al(8)	1.2696	−1.2224
N(9)	−1.2161	−18.4192	N(9)	−1.1616	−18.3901
N(10)	−0.7651	−18.4241	N(10)	−0.7699	−18.3855
Ga(11)	0.9972	−1.2552	Ga(11)	1.0024	−1.2392
N(12)	−1.0750	−18.4156	N(12)	−0.9475	−18.3842
Al(13)	1.2071	−1.2257	Al(13)	1.1771	−1.2418
N(14)	−0.7669	−18.4229	N(14)	−0.7570	−18.3896
Ga(15)	1.0015	−1.2544	Ga(15)	1.0088	−1.2358
N(16)	−0.6368	−18.3667	N(16)	−0.6195	−18.3231
N(17)	−0.6220	−18.3673	N(17)	−0.6003	−18.3222
-	-	-	H(18)	−0.0345	−1.1338

(c)

MnInGaN			MnInGaN–H		
Atom	Q	E_p	Atom	Q	E_p
Ga(1)	0.9511	−1.2550	Ga(1)	1.3172	−1.2338
N(2)	−1.0594	−18.4264	N(2)	−1.4501	−18.3901
In(3)	1.0827	−1.1292	In(3)	1.4791	−1.1137
N(4)	−1.0219	−18.4176	N(4)	−1.3388	−18.3983
Mn(5)	0.7195	−16.6614	Mn(5)	0.8126	−16.4568
Ga(6)	0.9420	−1.2549	Ga(6)	1.2959	−1.2328
N(7)	−1.0627	−18.4247	N(7)	−1.4452	−18.3922
In(8)	1.0981	−1.1280	In(8)	1.5085	−1.1173
N(9)	−1.0715	−18.4421	N(9)	−1.4269	−18.4351
N(10)	−0.7066	−18.4367	N(10)	−0.8648	−18.3712
Ga(11)	0.9750	−1.2612	Ga(11)	1.4177	−1.2144
N(12)	−0.9944	−18.4280	N(12)	−1.3611	−18.413
In(13)	1.0188	−1.1362	In(13)	1.3032	−1.1244
N(14)	−0.711	−18.4339	N(14)	−0.9195	−18.3859
Ga(15)	0.9812	−1.2596	Ga(15)	1.4087	−1.2201
N(16)	−0.5787	−18.3801	N(16)	−0.8417	−18.422
N(17)	−0.5623	−18.3807	N(17)	−0.8212	−18.4186
-	-	-	H(18)	−0.0735	−1.1254

3. RESULTS AND DISCUSSION

This investigation was based on first-principles studies and measured the electronic structure, optical prop-

erties, and thermoelectric properties of Mn doped GaN-based materials. It analyzed the effect of Mn impurities defects on the properties of GaN-based materials. In this article, the data was used to evaluate the efficiency of metal-doped hybrid nanoalloys of MnGaN, MnAlGaN, MnInGaN and their hydrated complexes of MnGaN–H, MnAlGaN–H, MnInGaN–H energy-saving in batteries.

3.1. Nuclear quadrupole resonance (NQR)

The "electric potential" through carrying over the electric charge was measured for MnGaN/ MnGaN–H, MnAlGaN/MnAlGaN–H, MnInGaN/ MnInGaN–H complexes (Table 1a,b,c).

Mn, Al, Ga, In, N and the hydrogen atom absorbed on MnGaN, MnAlGaN, MnInGaN have been calculated through the "Bader charge" and electronic potential properties. The values detect that with augmenting the negative charge of various atoms, the electric potential extracted from "NQR" calculations grows. Besides, the elements of N2, N4, N7, N9, N10, N12, N14 of MnGaN, MnAlGaN, MnInGaN have exhibited the most efficiency for admitting the electron from "electron donor" of H18 adsorbed on MnGaN, MnAlGaN, MnInGaN (Table 1a,b,c).

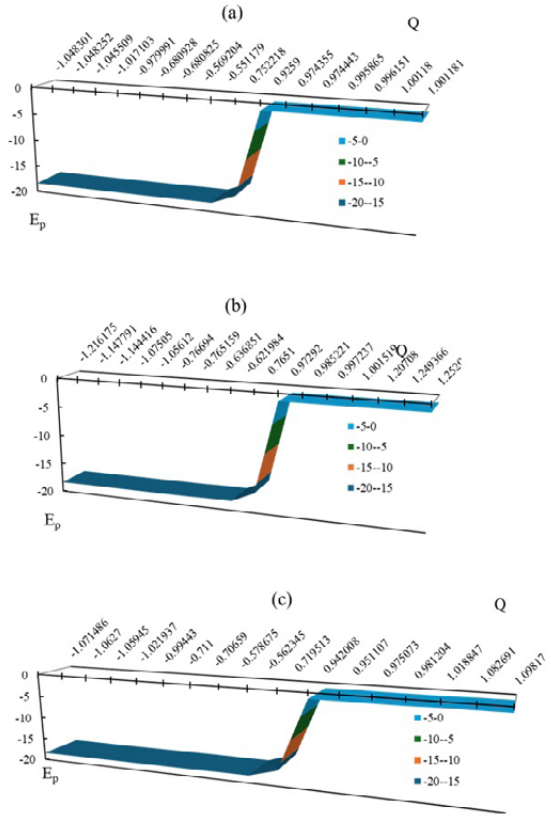

Figure 3. *"Electric potential" (E_p/a.u.) versus "Bader charge" (Q/coulomb) through "NQR" calculation for* **(a)** *MnGaN/MnGaN–H,* **(b)** *MnAlGaN/MnAlGaN–H, and* **(c)** *MnInGaN/MnInGaN–H nanoclusters.*

In Figure 3 (a,b,c), it has been drawn the electric potential versus Bader charge for Mn, Al, Ga, In, N and the hydrogen atom absorbed on MnGaN, MnAlGaN, MnInGaN. Therefore, it was observed the behavior of Mn, Ga and N atoms in MnGaN with high sensitivity based on relation coefficient of $R^2_{MnGaN} = 0.9095$; however, hydrogen adsorption on the MnGaN (MnGaN–H) has shown high sensitivity with relation coefficient of $R^2_{MnGaN-H} = 0.9897$ (Figure 3a). In Figure 3(b), it was observed the behavior of Mn, Al, Ga and N atoms in MnAlGaN and hydrogen adsorption on the MnAlGaN and formation of MnAlGaN–H with high sensitivity of $R^2_{MnAlGaN} = 0.8974$ and $R^2_{MnAlGaN-H} = 0.9548$, respectively.

The fluctuated peaks for electric potential have been shown around hydrogen adsorption on the MnInGaN which demonstrates the electron accepting specifications of hydrogen versus the Mn, In, Ga, N of MnInGaN and MnInGaN–H (Figure 3c). Based on the mentioned results, there can be renewed interest in combination of manganese, aluminum, gallium and indium in the nanoclusters of MnGaN, MnAlGaN, MnInGaN for potential applications in next-generation electronic devices.

3.2. Nuclear Magnetic Resonance (NMR) spectra

From the DFT calculations, it has been attained the chemical shielding (CS) tensors in the principal axes system to estimate the isotropic chemical-shielding (σ_{iso}) and anisotropic chemical-shielding (σ_{aniso}) [49]:

$$\sigma_{iso} = (\sigma_{11} + \sigma_{22} + \sigma_{33})/3 \quad (3);$$

$$\sigma_{aniso} = \sigma_{33} - (\sigma_{22} + \sigma_{11})/2 \quad (4)$$

The NMR data of isotropic (σ_{iso}) and anisotropic shielding tensors (σ_{aniso}) for Mn-doped GaN, AlGaN and InGaN and their hydrated derivatives of MnGaN–H, MnAlGaN–H, MnInGaN–H have been computed by Gaussian 16 revision C.01 program package [42] and been shown in Table 2 (a,b,c). The notable fragile signal intensity close to the parallel edge of the nanocluster sample might be owing to manganese binding induced non-spherical distribution of GaN (Figure 4a) and MnAlGaN (Figure 4b) heteroclusters. Figure 4 (c) exhibited the same tendency of shielding; however, a considerable deviation exists from doping atoms of manganese as electron acceptors on the surface of MnInGaN heterocluster.

Table 2. *Data of NMR shielding tensors (ppm) for selected atoms of* **(a)** *MnGaN/MnGaN–H,* **(b)** *MnAlGaN/MnAlGaN–H,* **(c)** *MnInGaN/MnInGaN–H heteroclusters.*

(a)

MnGaN			MnGaN–H		
Atom	σ_{iso}	σ_{aniso}	Atom	σ_{iso}	σ_{aniso}
Ga(1)	10.6772	8.1116	Ga(1)	7.8121	31.2686
N(2)	127.8331	150.7727	N(2)	11.3237	302.2757
Ga(3)	8.8962	7.1266	Ga(3)	0.0389	103.9122
N(4)	59.2200	255.8445	N(4)	518.4328	1015.7500
Mn(5)	1103.1944	682.7562	Mn(5)	61898.6207	83180.6883

Ga(6)	8.9005	7.1468	Ga(6)	2.0906	109.3062
N(7)	128.1480	149.7778	N(7)	45.0158	440.5489
Ga(8)	10.6774	8.0754	Ga(8)	5.6210	31.7011
N(9)	41.8262	220.7655	N(9)	445.6927	929.9371
N(10)	1008.9373	1461.3802	N(10)	3715.8543	8298.3128
Ga(11)	4.0487	15.5383	Ga(11)	0.2483	102.0391
N(12)	120.7217	362.2518	N(12)	367.1035	1288.8994
Ga(13)	2.2765	25.1952	Ga(13)	35.1872	123.5145
N(14)	1007.7725	1458.0491	N(14)	1857.1102	7832.5114
Ga(15)	4.0563	15.5221	Ga(15)	11.5119	73.3284
N(16)	120.6766	305.8095	N(16)	655.7327	1345.8956
N(17)	180.8583	320.6671	N(17)	1055.9230	1712.1127
-	-	-	H(18)	40.6176	502.4079

(b)

	MnAlGaN			MnAlGaN–H	
Atom	σ_{iso}	σ_{aniso}	Atom	σ_{iso}	σ_{aniso}
Ga(1)	10.4656	8.1593	Ga(1)	9.4127	57.4573
N(2)	146.5709	121.3465	N(2)	523.2930	1969.3799
Al(3)	7.3554	7.0508	Al(3)	3.9293	125.8000
N(4)	89.0872	176.7298	N(4)	1362.4308	2433.1374
Mn(5)	860.1968	607.8757	Mn(5)	44890.8709	68750.2634
Ga(6)	8.7556	6.9697	Ga(6)	14.4225	140.9499
N(7)	146.5804	115.6052	N(7)	367.1748	1905.4354
Al(8)	9.1447	9.2445	Al(8)	1.3642	33.6753
N(9)	97.5588	202.5538	N(9)	1645.6588	2817.2566
N(10)	1048.8518	1558.0300	N(10)	2093.5030	9430.3119
Ga(11)	3.0958	15.6767	Ga(11)	33.2386	113.4686
N(12)	94.3074	348.4218	N(12)	610.2133	1774.9398
Al(13)	4.1183	27.4952	Al(13)	10.8519	248.5418
N(14)	1063.7258	1561.8895	N(14)	3210.8323	7998.7947
Ga(15)	3.0675	15.6962	Ga(15)	26.8216	118.0277
N(16)	119.1640	317.7316	N(16)	336.4981	1962.7560
N(17)	171.0876	325.8904	N(17)	498.3192	5128.1686
-	-	-	H(18)	26.2759	347.0249

(c)

	MnInGaN			MnInGaN–H	
Atom	σ_{iso}	σ_{aniso}	Atom	σ_{iso}	σ_{aniso}
Ga(1)	9.8561	9.0718	Ga(1)	1.6742	42.3400
N(2)	141.2874	139.242	N(2)	43.0241	535.2459
In(3)	10.6228	6.0792	In(3)	16.1328	137.0235
N(4)	70.7476	185.3866	N(4)	1588.0044	3484.4781
Mn(5)	1100.8028	655.478	Mn(5)	75829.2468	87460.2786
Ga(6)	8.0587	6.4922	Ga(6)	12.6556	135.7235
N(7)	138.2746	141.262	N(7)	190.1028	374.0311
In(8)	11.5107	8.9599	In(8)	3.9630	42.2998
N(9)	76.7525	215.6169	N(9)	105.9158	687.9281
N(10)	1078.6734	1612.3978	N(10)	6052.6589	10061.7128
Ga(11)	2.4981	16.2989	Ga(11)	52.0566	69.7265
N(12)	101.3662	375.9026	N(12)	883.0356	2354.1239
In(13)	0.6973	25.46	In(13)	17.9037	85.9004
N(14)	1134.3858	1669.9935	N(14)	11759.9230	18294.7406
Ga(15)	1.9593	16.6879	Ga(15)	87.7874	114.0007
N(16)	129.6965	346.1977	N(16)	123.9797	695.5940
N(17)	189.0956	365.8149	N(17)	216.7121	726.1410
-	-	-	H(18)	91.2315	651.1319

The observed increase in the chemical shift anisotropy spans for nanocages of MnGaN/MnGaN–H (Figure 4a) and MnInGaN/MnInGaN–H (Figure 4c) is near N(10) and N(14), and for MnAlGaN/MnAlGaN–H is close to N(10), N(14), and N(17) (Figure 4b). The yield of electromagnetic shifting can be directed by the mentioned active nitrogen atoms extracted from hybrid nanomaterials. So, it can be observed that doped heteroclusters of MnGaN, MnAlGaN, or MnInGaN might ameliorate the capability of GaN-based nanocomposites in batteries for energy storage.

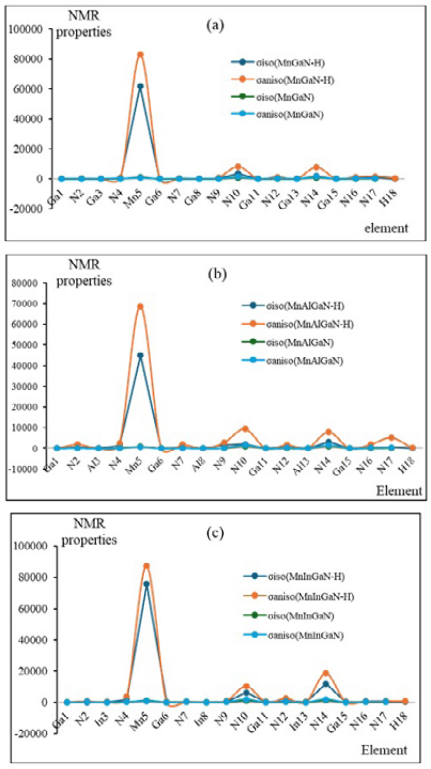

Figure 4. *The NMR properties of isotropic (σ_{iso}) and anisotropic (σ_{iso}) chemical shielding (ppm) for heteroclusters of* **(a)** *MnGaN/MnGaN–H,* **(b)** *MnAlGaN/MnAlGaN–H, and* **(c)** *MnInGaN/MnInGaN–H.*

3.3. Analysis of CDD, DOS/TDOS and ESP graphs

The amounts of charge density differences "CDD" is measured by considering isolated atoms or noninteracting ones. The mentioned approximation can be the lightest to use because the superposition value may be received from the primary status of the self-consistency cycle in the code that carries out the density functional theory (Figure5a,a', b,b', c,c') [50].

Figure5(a,a') indicates the atom of Mn5 from MnGaN and Mn5, H18 from MnGaN–H accompanying gallium and nitrogen atoms fluctuating around –9 to +3 Bohr. In Figure 5(b,b'), the atom of Mn5 from MnAlGaN and Mn5, H18 from MnAlGaN–H accompanying aluminum, gallium and nitrogen atoms have shown the fluctuation around –9 to +3 Bohr and –8 to +4 Bohr, respectively. Moreover, the atom of Mn5 from MnInGaN and Mn5, H18 from MnInGaN–H accompanying indium, gallium and nitrogen atoms have shown the fluctuation around –9 to +3 Bohr (Figure5c,c').

To better understand the different adsorption characteristics of MnGaN, MnGaN–H, MnAlGaN, MnAlGaN–H, MnInGaN, MnInGaN–H, total density of states (TDOS) using Multiwfn program [51,52] has been measured.

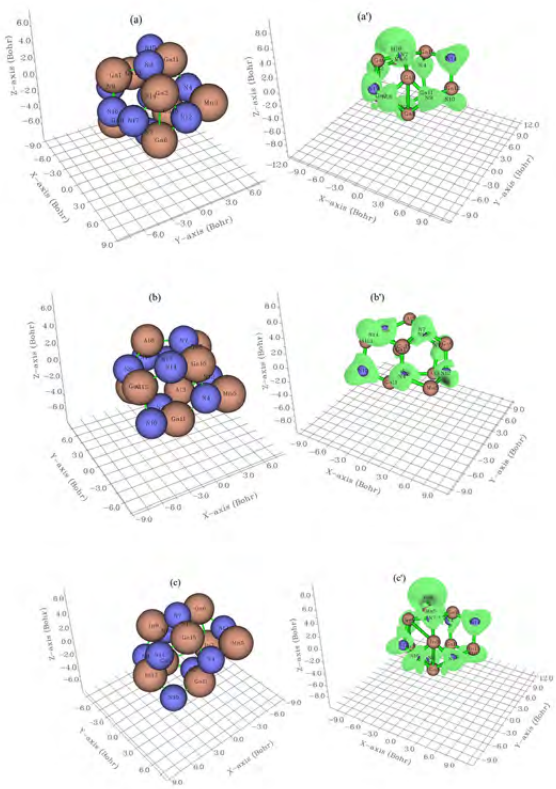

Figure 5. *Charge density differences "CDD" graphs for heteroclusters through hydrogen adsorption including* **(a)** *MnGaN,* **(a')** *MnGaN–H,* **(b)** *MnAlGaN,* **(b')** *MnAlGaN–H,* **(c)** *MnInGaN,* **(c')** *MnInGaN–H.*

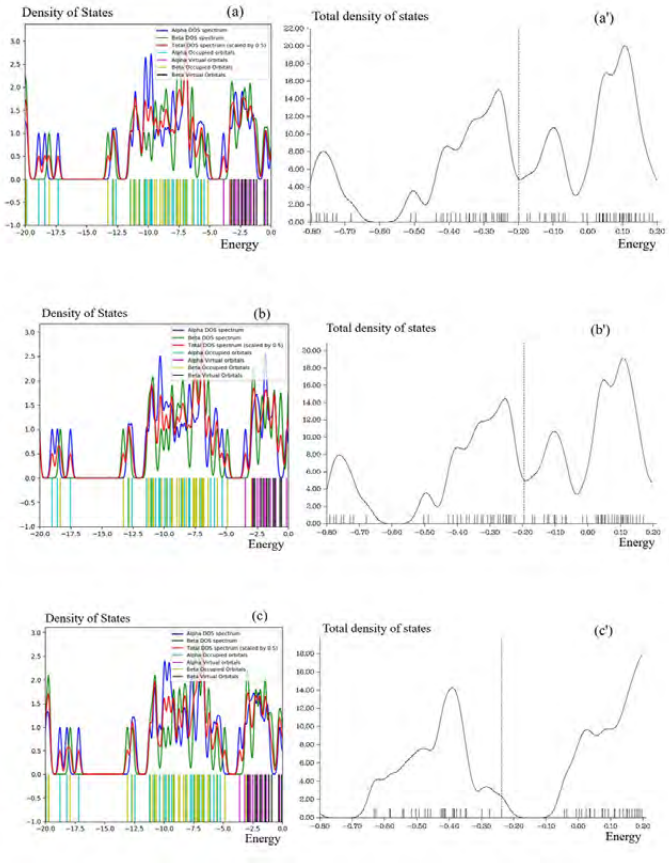

Figure 6. *DOS/TDOS graphs of heteroclusters include* **(a)** *MnGaN,* **(a')** *MnGaN–H,* **(b)** *MnAlGaN,* **(b')** *MnAlGaN–H,* **(c)** *MnInGaN,* **(c')** *MnInGaN–H.*

This parameter can indicate the existence of important chemical interactions often on the convex side (Figure 6a,a', b,b', c,c'). In isolated system (such as molecule), the energy levels are discrete, the concept of density of state (DOS) is supposed completely valueless in this situation. Therefore, the original total DOS (TDOS) of isolated system can be written as [53]:

$$TDOS\ (E) = \sum_i \delta\ (E - \epsilon_i\ )\ \ (5)$$

$$G(x) = \frac{1}{c\sqrt{2\pi}} e^{-\frac{x^2}{2c^2}} \quad \text{where} \quad c = \frac{\text{FWHM}}{2\sqrt{2\ln x}}\ \ (6)$$

In the TDOS map, each discrete vertical line corresponds to a molecular orbital (MO), the dashed line highlights the position of HOMO. The curve is the TDOS simulated based on the distribution of MO energy levels. In the negative part, the region around −0.40 a.u. has obviously larger state density than other regions for MnGaN, MnGaN–H, MnAlGaN, MnAlGaN–H, MnInGaN, MnInGaN–H (Figure 6a,a', b,b', c,c'). However, MnInGaN–H (Figure 6c') has shown larger state density through pointed peaks than MnGaN–H (Figure 6a') and MnAlGaN–H (Figure 6b'). It is remarkable that the excessive growth technique on doping manganese as noble transition metal is a potential approach to designing high efficiency hybrid semipolar gallium nitride alloys devices on aluminum or indium layers in a long wavelength zone.

This function measures the electrostatic interaction between a unit point charge placed at **r** and the system of interest. A positive (negative) value implies that the current position is dominated by nuclear (electronic) charges. Molecular electrostatic potential (ESP) has been widely used for prediction of nucleophilic and electrophilic sites for a long time. It is also valuable in studying hydrogen bonds, halogen bonds, molecular recognitions and the intermolecular interaction of aromatics [54].

$$V_{tot}(r) = V_{nuc}(r) + V_{ele}(r) = \sum_A \frac{Z_A}{|r - R_A|} - \int \frac{\rho(r')}{|r - r'|} dr'\ \ (7)$$

Z_A is nuclear charge, if pseudopotential is used, then Z_A is the number of explicitly expressed electrons. Notice that evaluating ESP is much more time-consuming than evaluating other functions. Also note that ESP in Multiwfn is evaluated exactly by nuclear attractive integrals rather than using approximate methods (such as multipole expansion, numerical Poisson equation), hence you may find the results generated by Multiwfn are somewhat different from those outputted by other quantum chemistry codes. In order to speed up ESP evaluation, Multiwfn ignores some integrals that have little contributions. The threshold for ignoring is controlled by "esppreccutoff" in settings.ini, enlarging this parameter results in more accurate ESP value, but also brings more computational cost. The ESP evaluated under default value is accurate enough in general cases.

The nanoclusters of MnGaN/MnGaN–H (Figure 7a,a'), MnAlGaN/MnAlGaN–H (Figure 7b,b') and MnInGaN/MnInGaN–H (Figure 7c,c') can be defined by ESP graphs owing to exploring their delocalization/localization characterizations of electrons and chemical bonds. Covalent zones have high ESP value, the electron depletion zones between valence shell and inner shell are indicated by the blue circles around nuclei.

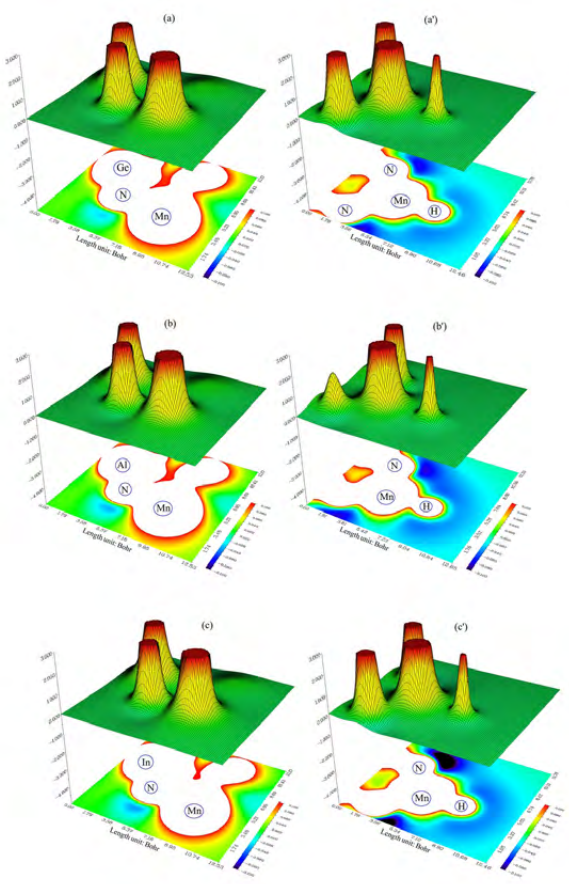

Figure 7. *The Counter line map of ESP for* **(a)** *MnGaN,* **(a')** *MnGaN–H,* **(b)** *MnAlGaN,* **(b')** *MnAlGaN–H,* **(c)** *MnInGaN and* **(c')** *MnInGaN–H.*

Hydration of Mn-doped GaN, AlGaN, InGaN indicates a larger isosurface map of electron delocalization due to labeling atoms of N(4), Mn (5), H (18) in MnGaN–H (Figure 7a'), MnAlGaN–H (Figure 7b'), MnInGaN–H (Figure 7c'). A narrower connected area occupied by an isosurface map means that electron delocalization is relatively difficult. However, the large counter map of ESP for MnGaN, MnAlGaN, MnInGaN can confirm that doping Mn nanoparticles on the surface increases the efficiency of batteries of GaN, AlGaN, InGaN for energy storage. In fact, the counter map of ESP can confirm that MnGaN, MnAlGaN, MnInGaN nanoclusters with labeling atoms increase the efficiency during hydrogen adsorption.

Moreover, intermolecular orbital overlap integral is important in discussions of intermolecular charge transfer which can calculate HOMO-HOMO and LUMO-LUMO overlap integrals between the hydrogen atom and hybrid heteroclusters of MnGaN, MnAlGaN, MnInGaN. The wavefunction level we used is CAM–B3LYP–D3/6–311+G(d,p) that correspond to HOMO and LUMO, respectively (Table 3).

Table 3. *LUMO/HOMO, energy gap (ΔE) and overlap integral for MnGaN, MnGaN–H, MnAlGaN, MnAlGaN–H, MnInGaN, MnInGaN–H.*

Heteroclusters	E_{LUMO} (a.u.)	E_{HOMO} (a.u.)	$\Delta E=E_{LUMO}-E_{HOMO}$ (a.u.)	$< S^2 >$
MnGaN				4.5498
MnGaN–H	−0.1749	−0.1995	0.0246	
MnAlGaN				4.6091
MnAlGaN–H	−0.1703	−0.1953	0.0249	
MnInGaN				4.5186
MnInGaN–H	−0.0423	−0.2368	0.1945	

For unrestricted wavefunctions, orthonormalization condition does not hold in general between alpha and beta orbitals. This function computes the overlap matrix between alpha and beta orbitals:

$$S_{i,j}^{\alpha,\beta} = \int \varphi_i^{\alpha}(r)\varphi_j^{\beta}(r)dr \quad (8)$$

The diagonal elements are useful for evaluating the matching degree of corresponding spin orbital pairs, evident deviation to 1 indicates that spin polarization is remarkable. Because the expectation of S^2 operator for single determinant (SD) wavefunction can be easily derived from the matrix, Multiwfn [51,52] outputs this quantity together:

$$< S^2 >_{SD} = < S^2 >_{Exact} + N^{\beta} - \sum_i^{N^{\alpha}} \sum_j^{N^{\beta}} \left| S_{i,j}^{\alpha,\beta} \right|^2 \quad (9)$$

where $< S^2 >$ is the exact value of square of total spin angular momentum:

$$< S^2 >_{Exact} = \frac{N^{\alpha}-N^{\beta}}{2}\left(\frac{N^{\alpha}-N^{\beta}}{2}+1\right) \quad (10)$$

A strategy for increasing the square of an overlap integral ($< S^2 >$) of electron in MnGaN, MnAlGaN, MnInGaN is proposed by doping of Mn atom (Table 3). Therefore, E_{LUMO} (a.u.), E_{LUMO} (a.u.) and the local bandgap energies (ΔE/a.u.) and immobile charges induced by polarization discontinuity are simultaneously controlled throughout the structures, and optimized band profiles are eventually achieved for MnGaN, MnGaN–H, MnAlGaN, MnAlGaN–H, MnInGaN, MnInGaN–H (Table 3). $<S^2>$ has been ameliorated after doping the transition metals atom of manganese on the surface of GaN and the ternary alloys of AlGaN and InGaN for that might increase electron charge transfer in superconductor devices.

The amount of "Mayer bond order" [55] is generally according to empirical bond order for the single bond is near 1.0. "Mulliken bond order" [56] with a small accord with empirical bond order is not appropriate for quantifying bonding strength, for which Mayer bond order always performs better. However, "Mulliken bond order" is a good qualitative indicator for "positive amount" of bonding and "negative amount" of antibonding which are evacuated and localized, respectively (Table 4).

As it is seen in Table 4, "Laplacian bond order" [57] has a straight cohesion with bond polarity, bond dissociation energy and bond vibrational frequency. The low value of Laplacian bond order might demonstrate that it is insensitive to the calculation degree applied for producing electron density. Generally, the value of "Fuzzy bond order" is near Mayer bond order, especially for low-polar bonds, but much more stable with respect to the change in basis-set. Computation of "Fuzzy bond order" demands running "Becke's DFT" numerical integration, owing to which the calculation value is larger than assessment of "Mayer bond order" and it can concede more precisely [58].

Table 4. *The bond order of Mayer, Wiberg, Mulliken, Laplacian and Fuzzy from mixed alpha and beta density matrix for hydrated hetero-clusters of MnGaN–H, MnAlGaN–H, MnInGaN–H.*

Hetero clusters	Mayer	Wiberg	Mulliken	Laplacian	Fuzzy
MnGaN–H	0.9423	0.9311	0.6627	0.0995	0.9477
MnAlGaN–H	0.9359	0.9225	0.6483	0.1001	0.9354
MnInGaN–H	0.9635	0.9514	0.7323	0.1522	0.9614

3.4. Infrared spectroscopy & thermochemistry

The infrared spectroscopy (IR) has been performed for nanocomposites of MnGaN/ MnGaN–H (Figure8a,a'), MnAlGaN/ MnAlGaN–H (Figure8b,b'), and MnInGaN/MnInGaN–H (Figure8c,c') through hydrogen adsorption.

The frequency value through the IR curves between 200–1000 cm^{-1} for MnGaN with one sharp peak around 414.78 cm^{-1} (Figure 8a) has been shifted to two pointed peaks around 863.78 and 921.24 cm^{-1} of MnGaN–H (Figure 8a'). However, Figure 8(b) shows two sharp peaks around 389.02 and 713.88 cm^{-1} for MnAlGaN that have been shifted to one sharp peak around 952.45 cm^{-1} for MnAlGaN–H (Figure 8b'). Furthermore, Figure 8(c) indicates one sharp peak around 366.88 cm^{-1} for MnInGaN that have been shifted to several sharp peaks around 640.30, 767.66, 783.92 and 1311.73 cm^{-1} for MnInGaN–H (Figure 8c')

Energy storage with heteroclusters has described that the frame of the overcoming cluster is related to MnGaN–H, MnAlGaN–H, and MnInGaN–H in the high amounts of frequency. This property makes these hybrid nanomaterials potentially advantageous for certain high-frequency applications requiring batteries for energy storage. The advantages of manganese over GaN, AlGaN, or InGaN include its higher electron and hole mobility, allowing manganese doping devices to operate at higher frequencies than non-doping devices.

Table 5 through the thermodynamic specifications concluded that heteroclusters of MnGaN, MnGaN–H, MnAlGaN, MnAlGaN–H, MnInGaN, MnInGaN–H might be more efficient structure for energy storage in the batteries.

Thermodynamic parameters of heteroclusters of MnGaN/MnGaN–H, MnAlGaN/MnAlGaN–H, and MnInGaN/MnInGaN–H have been assigned (Table 5). The changes of Gibbs free energy versus for all nanocomposites could detect the maximum efficiency of MnAlGaN–H> MnGaN–H> MnInGaN–H for energy storage in the batteries through (Table 5).

Table 5. *The thermodynamic characters of MnGaN, MnGaN–H, MnAlGaN, MnAlGaN–H, MnInGaN, MnInGaN–H nanoclusters using CAM–B3LYP–D3/6–311+G(d, p) calculation*

Compound	Dipole moment (Debye)	$\Delta E^{o}_{ads} \times 10^{-3}$ (kcal/mol)	$\Delta H^{o}_{ads} \times 10^{-3}$ (kcal/mol)	$\Delta G^{o}_{ads} \times 10^{-3}$ (kcal/mol)	$E^{o}_{H-binding}$ (kcal/mol)
MnGaN	4.8247	–383.439	–383.439	–383.483	-
MnGaN –H	7.3741	–383.596	–383.595	–383.636	–157
MnAlGaN	4.7914	–383.095	–383.094	–383.136	-
MnAlGaN –H	7.3741	–383.596	–383.595	–383.636	–501
MnInGaN	7.3629	–383.035	–383.035	–383.082	-
MnInGaN –H	4.3037	–383.472	–383.472	–383.513	–437

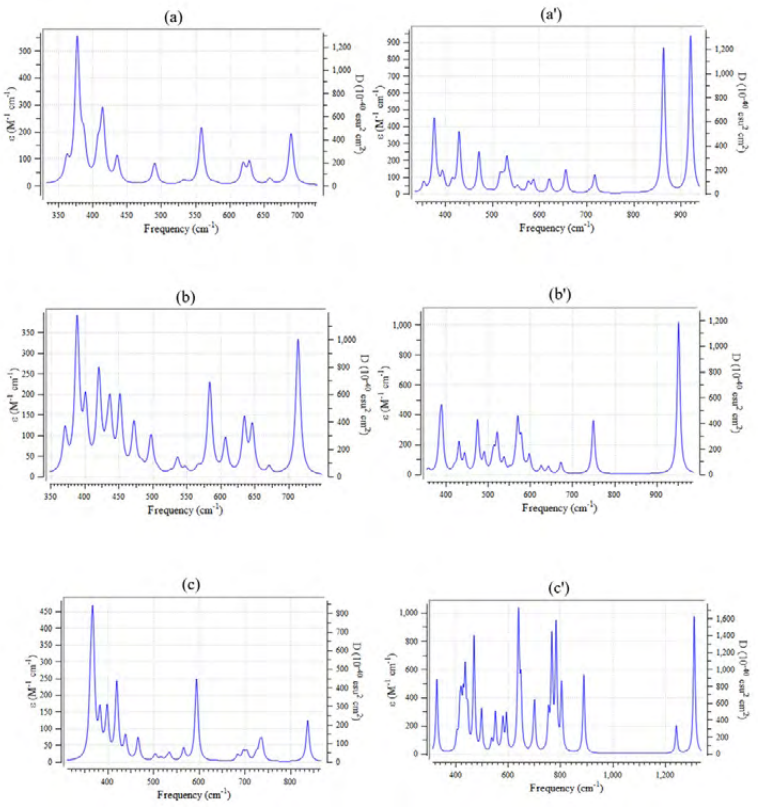

Figure 8. *Frequency (cm^{-1}) changes through the IR spectra for heteroclusters of* **(a)** *MnGaN,* **(a')** *MnGaN–H,* **(b)** *MnAlGaN,* **(b')** *MnAlGaN–H, and* **(c)** *MnInGaN,* **(c')** *MnInGaN–H.*

The adsorption efficiency of MnGaN–H, MnAlGaN–H, MnInGaN–H based on dipole moment has been evaluated by the . The batteries formed by MnGaN, MnAlGaN, MnInGaN feature a hierarchical structure with the electron donor/acceptor layer sandwiched by anode and cathode, which raises the importance of controlling the molecular crystal orientation, domain size, and vertical distribution to facilitate the charge collection at electrodes. In this paper, we have demonstrated that the nanocomposite semiconductor of gallium nitride-based structure can lead to a significant absorption enhancement in a broad spectral range of incident light in the presence of aluminum, indium and manganese. A comparison between batteries containing 3d transition metal of Mn-doped GaN, AlGaN, InGaN shows that a transistor containing these elements shows a more enhanced cell performance than the cells containing only the bare gallium nitride-based structure. This efficient doping strategy not only bridges the gaps of heteroatom doped GaN-based semiconductor materials, but also can provide deep insights into controlling the electrical and optical properties of these doping hybrid nanoclusters. According to the first-principles study, it was systematically studied the stability and optoelectronic properties of the GaN monolayer pre-doping and post-doping. Doping with Mn is studied, confirming structural stability and altered electronic properties. Doped systems show spin polarization and reduced bandgaps, while the optical properties reveal changes in dielectric functions and enhanced absorption coefficients, particularly in the IR region for GaN and its derivatives.

4. CONCLUSION

Manganese doping can transform GaN materials into p-type semiconductors, which is crucial for achieving p-n junctions or p-type layers in GaN based electronic devices. In addition, the optical properties and thermoelectric properties of different GaN doping models were calculated. Hydrogen grabbing on the heteroclusters of Mn-doped GaN, AlGaN, InGaN as batteries was investigated by first-principles calculations. We have provided gallium nitride-based semiconductors which are doped with manganese. The geometrical parameters of doping manganese on the surface of GaN, AlGaN, InGaN through the absorption status and current charge density of the batteries was studied. Thermodynamic parameters have constructed a detailed molecular model for atom–atom interactions and a distribution of point charges which can be utilized to reproduce the polarity of the solid material and the adsorbing molecules. Energy storage with heteroclusters has described that the frame of the overcoming cluster is related to MnGaN, MnAlGaN or MnInGaN in the high amounts of frequency. This property makes MnGaN, MnAlGaN or MnInGaN potentially advantageous for certain high-frequency applications requiring batteries for energy storage due to hydrogen adsorption by formation of MnGaN–H, MnAlGaN–H or MnInGaN–H. The advantages of manganese over GaN, AlGaN, or InGaN include its higher electron and hole mobility, allowing manganese doping devices to operate at higher frequencies than non-doping devices. These findings highlight the controllability and variability of the band gap in GaN-based semiconductors, providing new potential applications for GaN as a material in optoelectronic devices and batteries.

REFERENCES

1. M. L. Nakarmi, N. Nepal, J. Y. Lin and H. X. Jiang, Photoluminescence studies of impurity transitions in Mg-doped AlGaN alloys. Appl. Phys. Lett., 2009, 94, 091903.
2. K. B. Nam, J. Li, M. L. Nakarmi, J. Y. Lin and H. X. Jiang, Unique optical properties of AlGaN alloys and related ultraviolet emitters. Appl. Phys. Lett., 2002, 81, 1038–1040.
3. J. P. Zhang, X. Hu, Y. Bilenko, J. Deng, A. Lunev, M. S. Shur, R. Gaska, M. Shatalov, J. W. Yang and M. A. Khan, AlGaN-based 280 nm light-emitting diodes with continuous-wave power exceeding at 1mW at 25 mA. Appl. Phys. Lett., 2004, 85, 5532–5534.
4. Z. G. Shao, D. J. Chen, H. Lu, R. Zhang, D. P. Cao, W. J. Luo, Y. D. Zheng, L. Li and Z. H. Li, High-Gain AlGaN Solar-Blind Avalanche Photodiodes. IEEE Electron Device Lett., 2014, 35, 372–374.
5. Mollaamin, F., Monajjemi, M. In Silico-DFT Investigation of Nanocluster Alloys of Al-(Mg, Ge, Sn) Coated by Nitrogen Heterocyclic Carbenes as Corrosion Inhibitors. *J Clust Sci* **34**, 2901–2918 (2023). https://doi.org/10.1007/s10876-023-02436-5
6. Liu, S., Ye, C., Cai, X. et al. Performance enhancement of AlGaN deep-ultraviolet light-emitting diodes with varied superlattice barrier electron blocking layer. Appl. Phys. A 122, 527 (2016). https://doi.org/10.1007/s00339-016-0073-0.
7. J. Simon, V. Protasenko, C. Lian, H. Xing and D. Jena, Polarization-induced hole doping in wide-band-gap uniaxial semiconductor heterostructures. Science, 2010, 327, 60–64.
8. Mollaamin, F. and Monajjemi, M. Graphene-based resistant sensor decorated with Mn, Co, Cu for nitric oxide detection: Langmuir adsorption & DFT method. *Sensor Review*, 43(4), 266-279 (2023). https://doi.org/10.1108/SR-03-2023-0040
9. Jinn-Kong Sheu, Po-Cheng Chen, Cheng-Lun Shin, Ming-Lun Lee, Po-Hsun Liao, Wei-Chih Lai, Manganese-doped AlGaN/GaN heterojunction solar cells with intermediate band absorption. Solar Energy Materials and Solar Cells. 157, 727–732 (2016). doi.org/10.1016/j.solmat.2016.07.047
10. Jinn-Kong Sheu; Feng-Wen Huang; Chia-Hui Lee; Ming-Lun Lee; Yu-Hsiang Yeh; Po-Cheng Chen; Wei-Chih Lai, Improved conversion efficiency of GaN-based solar cells with Mn-doped absorption layer. Appl. Phys. Lett. 103, 063906 (2013). https://doi.org/10.1063/1.4818340
11. A. Martí, C. Tablero, E. Antolín, A. Luque, R.P. Campion, S.V. Novikov, C.T. Foxon, Potential of Mn doped In1–xGaxN for implementing intermediate band solar cells. Solar Energy Materials and Solar Cells. 93(5), 641-644 (2009). https://doi.org/10.1016/j.solmat.2008.12.031
12. Wu J, Walukiewicz W, Yu KM, et al. Superior radiation resistance of $In_{1-x}Ga_xN$ alloys: full-solar-spectrum photovoltaic material system. *J Appl Phys*. 2003; **94**: 6477-6482.
13. Wu J, Walukiewicz W, Yu K, et al. Small band gap bowing in $In_{1-x}Ga_xN$ alloys. *Appl Phys Lett*. 2002; **80**: 4741-4743.
14. Singh R, Doppalapudi D, Moustakas TD, Romano LT. Phase separation in InGaN thick films and formation of InGaN/GaN double heterostructures in the entire alloy composition. *Appl Phys Lett*. 1997; **70**: 1089-1091.
15. Lien DH, Hsiao YH, Yang SG, et al. Harsh photovoltaics using InGaN/GaN multiple quantum well schemes. *Nano Energy*. 2015; **11**: 104-109.
16. Kuwahara Y, Fujii T, Fujiyama Y, et al. Realization of nitride-based solar cell on freestanding GaN substrate. *Appl Phys Express*. 2010; **3**: 111001-1-111001-3.
17. Fatemeh Mollaamin, Design, Functionalization, and Characterization of InGaN Nanocluster for Energy Storage in Solar Cell Basics: A Quantum Chemistry Study. Materials International. 7(1), 2025, 3. https://doi.org/10.33263/Materials71.003
18. Neufeld CJ, Cruz SC, Farrell RM, et al. Effect of doping and polarization on carrier collection in InGaN quantum well solar cells. *Appl Phys Lett*. 2011; **98**: 243507-1-243507-3.

19. Shen H, Maes B. Combined plasmonic gratings in organic solar cells. *Opt Express*. 2011;19: A1202-A1210.
20. Wang KX, Yu Z, Liu V, Cui Y, Fan S. Absorption enhancement in ultrathin crystalline silicon solar cells with antireflection and light-trapping nanocone gratings. *Nano Lett*. 2012; 12: 1616-1619.
21. Meng X, Drouard E, Gomard G, Peretti R, Fave A, Seassal C. Combined front and back diffraction gratings for broad band light trapping in thin film solar cell. *Opt Express*. 2012; 20: A560-A571.
22. Abass A, Le KQ, Alu A, Burgelman M, Maes B. Dual-interface gratings for broadband absorption enhancement in thin-film solar cells. *Phys Rev B*. 2012; 85:115449-1-115449-8.
23. Chriki R, Yanai A, Shappir J, Levy U. Enhanced efficiency of thin film solar cells using a shifted dual grating plasmonic structure.*Opt Express*. 2013;21: A382-A391.
24. Hsu WC, Tong JK, Branham MS, et al. Mismatched front and back gratings for optimum light trapping in ultra-thin crystalline silicon solar cells. *Opt Commun*. 2016; 377: 52-58.
25. Isabella O, Vismara R, Ingenito A, Rezaei N, Zeman M. Decoupled front/back dielectric textures for flat ultra-thin c-Si solar cells. *Opt Express*. 2016; 24: A708-A719.
26. Jing Lin, Yuefeng Yu, Zhenzhu Xu, Fangliang Gao, Zhijie Zhang, Fanyi Zeng, Wenliang Wang, Guoqiang Li, Electronic engineering of transition metal Zn-doped InGaN nanorods arrays for photoelectrochemical water splitting, Journal of Power Sources, 450, 227578 (2020), https://doi.org/10.1016/j.jpowsour.2019.227578.
27. Uttam K. Kumawat, Kamal Kumar, Priyanka Bhardwaj, Anuj Dhawan, Indium-rich InGaN/GaN solar cells with improved performance due to plasmonic and dielectric nanogratings. 7(6), 2469-2482 (2019). https://doi.org/10.1002/ese3.436.
28. Mollaamin, F. Competitive Intracellular Hydrogen-Nanocarrier Among Aluminum, Carbon, or Silicon Implantation: a Novel Technology of Eco-Friendly Energy Storage using Research Density Functional Theory. *Russ. J. Phys. Chem. B* **18**, 805–820 (2024). https://doi.org/10.1134/S1990793124700131
29. Zadeh MAA, Lari H, Kharghanian L, et al. Density Functional Theory Study and Anti-Cancer Properties of Shyshaq Plant: In View Point of Nano Biotechnology. Journal of Computational and Theoretical Nanoscience. 2015; 12(11): 4358-4367. doi: 10.1166/jctn.2015.4366
30. Mollaamin, F., Monajjemi, M. (2024). Designing novel nanomaterials for Li-ion batteries: A physico-chemical study through hydrogen-powered horizons. New Materials, Compounds and Applications, 8(3), 303-323 https://doi.org/10.62476/nmca83303
31. Mollaamin, F., Monajjemi, M. Tailoring and functionalizing the graphitic-like GaN and GaP nanostructures as selective sensors for NO, NO_2, and NH_3 adsorbing: a DFT study. *J Mol Model* **29**, 170 (2023). https://doi.org/10.1007/s00894-023-05567-8
32. Mollaamin, F., Monajjemi, M. Transition metal (X = Mn, Fe, Co, Ni, Cu, Zn)-doped graphene as gas sensor for CO_2 and NO_2 detection: a molecular modeling framework by DFT perspective. *J Mol Model* **29**, 119 (2023). https://doi.org/10.1007/s00894-023-05526-3
33. Tahan, A., Mollaamin, F. & Monajjemi, M. Thermochemistry and NBO analysis of peptide bond: Investigation of basis sets and binding energy. *Russ. J. Phys. Chem.* **83**, 587–597 (2009). https://doi.org/10.1134/S003602440904013X
34. M. Monajjemi, M. Jafari Azan &F. Mollaamin, Density Functional Theory Study on B30N20 Nanocage in Structural Properties and Thermochemical Outlook. Fullerenes, Nanotubes and Carbon Nanostructures. 21(6) 2013, 503-515. https://doi.org/10.1080/1536383X.2011.629762
35. F. Mollaamin, M. Monajjemi, Molecular modelling framework of metal-organic clusters for conserving surfaces: Langmuir sorption through the TD-DFT/ONIOM approach. Molecular Simulation 49 (4), 2023, 365-376. https://doi.org/10.1080/08927022.2022.2159996
36. K. Kim; K. D. Jordan (1994). Comparison of Density Functional and MP2 Calculations on the Water Monomer and Dimer. J. Phys. Chem. 98 (40): 10089–10094. doi:10.1021/j100091a024.
37. Mollaamin, F., Shahriari, S., Monajjemi, M. *et al.* Nanocluster of Aluminum Lattice via Organic Inhibitors Coating: A Study of Freundlich Adsorption. *J Clust Sci* **34**, 1547–1562 (2023). https://doi.org/10.1007/s10876-022-02335-1
38. Ghalandari B, Monajjemi M, Mollaamin F. Theoretical investigation of carbon nanotube binding to DNA in view of drug delivery. J Comput Theor Nanosci. 2011; 8(7): 1212-1219. doi:10.1166/jctn.2011.1801
39. Mollaamin, F., Monajjemi,M., Adsorption ability of Ga_5N_{10} nanomaterial for removing metal ions contamination from drinking water by DFT, Int J Quantum Chem, 2024, 124, e27348. https://doi.org/10.1002/qua.27348.
40. Mollaamin F and Monajjemi M. Molecular modelling framework of metal-organic clusters for conserving surfaces: Langmuir sorption through the TD-DFT/ONIOM approach. MOLECULAR SIMULATION 2023; 49(4): 365–376. https://doi.org/10.1080/08927022.2022.2159996.
41. S. H. Vosko; L. Wilk; M. Nusair (1980). Accurate spin-dependent electron liquid correlation energies for local spin density calculations: a critical analysis. Can. J. Phys. 58 (8): 1200–1211. Bibcode:1980CaJPh.58.1200V. doi:10.1139/p80-159.
42. Frisch, M. J.; Trucks, G. W.; Schlegel, H. B.; Scuseria, G. E.; Robb, M. A.; et al. Gaussian 16, Revision C.01, Gaussian, Inc., Wallingford CT, 2016.
43. GaussView, Version 6.06.16, Dennington, Roy; Keith, Todd A.; Millam, John M. Semichem Inc., Shawnee Mission, KS, 2016.
44. Trontelj, Z.; Pirnat, J.; Jazbinšek, V.; Lužnik, J.; Srčič, S.; Lavrič, Z.; Beguš, S.; Apih, T.; Žagar, V.; Seliger, J. Nuclear Quadrupole Resonance (NQR)—A Use-

ful Spectroscopic Tool in Pharmacy for the Study of Polymorphism. Crystals 2020, 10, 450. https://doi.org/10.3390/cryst10060450.
45. Sciotto, R.; Ruiz Alvarado, I.A.; Schmidt, W.G. Substrate Doping and Defect Influence on P-Rich InP(001):H Surface Properties. Surfaces 2024, 7, 79-87. https://doi.org/10.3390/surfaces7010006.
46. Monajjemi M, Afsharnezhad S, Jaafari MR, Mirdamadi S, Mollaamin F, Monajemi H, Investigation of energy and NMR isotropic shift on the internal rotation Barrier of Θ4 dihedral angle of the DLPC: A GIAO study. Chemistry. 2008; 17(1): 55-69.
47. Young, Hugh A.; Freedman, Roger D. (2012). Sears and Zemansky's University Physics with Modern Physics (13th ed.). Boston: Addison-Wesley. p. 754.
48. Bakhshi, K.; Mollaamin, F.; Monajjemi, M. Exchange and Correlation Effect of Hydrogen Chemisorption on Nano V(100) Surface: A DFT Study by Generalized Gradient Approximation (GGA). J Comput Theor Nanosci. 2011, 8(4), 763-768. https://doi.org/10.1166/jctn.2011.1750
49. Sarasia EM, Afsharnezhad S, Honarparvar B, et al. Theoretical study of solvent effect on NMR shielding tensors of luciferin derivatives. Physics and Chemistry of Liquids. 2011; 49(5): 561-571. doi: 10.1080/00319101003698992
50. Zihan Xu, Chenglong Qin, Yushu Yu, Gang Jiang, Liang Zhao, First-principles study of adsorption, dissociation, and diffusion of hydrogen on α-U (110) surface. AIP Advances 14, 055114 (2024). https://doi.org/10.1063/5.0208082
51 Tian Lu, Feiwu Chen, Multiwfn: A multifunctional wavefunction analyzer. J. Comput. Chem. 33, 580-592 (2012). https://doi.org/10.1002/jcc.22885.
52. Tian Lu, A comprehensive electron wavefunction analysis toolbox for chemists, Multiwfn. *J. Chem. Phys.* 161, 082503 (2024). https://doi.org/10.1063/5.0216272.
53. Becke, A. D. Edgecombe, K. E. A simple measure of electron localization in atomic and molecular systems, J. Chem. Phys. 9(1990)5397–5403. https://doi.org/10.1063/1.458517
54. Jane S. Murray, Peter Politzer, The electrostatic potential: an overview. WIREs Comput. Mol. Sci., 1(2), 153-163 (2011). https://doi.org/10.1002/wcms.19.
55. I. Mayer, Improved definition of bond orders for correlated wave functions. Chemical Physics Letters 544, 83-86 (2012). https://doi.org/10.1016/j.cplett.2012.07.0
56. Mollaamin, F., Baei, M.T., Monajjemi, M. *et al.* A DFT study of hydrogen chemisorption on V (100) surfaces. *Russ. J. Phys. Chem.* **82**, 2354–2361 (2008). https://doi.org/10.1134/S0036024408130323
57. Tian Lu and Feiwu Chen, Bond Order Analysis Based on the Laplacian of Electron Density in Fuzzy Overlap Space. J. Phys. Chem. A 2013, 117, 14, 3100–3108. https://doi.org/10.1021/jp4010345
58. Wang, X.; Zhang, X.; Pedrycz, W.; Yang, S.-H.; Boutat, D. Consensus of T-S Fuzzy Fractional-Order, Singular Perturbation, Multi-Agent Systems. *Fractal Fract.* **2024**, *8*, 523. https://doi.org/10.3390/fractalfract8090523